Ultra-broadband and polarization-independent planar absorber based on multilayered graphene*

Jiao Wang(王娇)[1], Chao-Ning Gao(高超宁)[1], Yan-Nan Jiang(姜彦南)[1,2,†], and Charles Nwakanma Akwuruoha[3]

[1] *Guangxi Key Laboratory of Wireless Wideband Communication and Signal Processing, Guilin* 541004, *China*
[2] *Key Laboratory of Cognitive Radio and Information Processing (Ministry of Education), Guilin University of Electronic Technology, Guilin* 541004, *China*
[3] *School of Electrical and Electronic Engineering, University of Manchester, Manchester, M*13 9*PL, UK*

(Received 9 May 2017; revised manuscript received 8 June 2017; published online 30 September 2017)

We propose an ultra-broadband and polarization independent planar absorber comprising multilayered graphene. The bandwidth of the proposed absorber is extended by increasing the number of layers of graphene, and it is polarization independent due to its symmetrical unit structure. The full wave simulation results show that an absorber with three graphene-based layers can efficiently harvest an electromagnetic wave with random polarization from 17.9 GHz to 188.7 GHz (i.e., covering frequency regimes from K to D bands and relative bandwidth of $\sim$ 165%). The physical absorption mechanism of ultra-broadband absorption has been elaborated upon using the destructive interference method and multiple resonances approach in a multilayered medium. The proposed absorber can be used in many applications such as medical treatment, electromagnetic compatibility, and stealth technique.

Keywords: multilayered graphene absorber, ultra-broadband, polarization independent

PACS: 41.20.Jb, 52.25.Os, 73.22.Pr **DOI:** 10.1088/1674-1056/26/11/114102

1. Introduction

Absorbers can be used in applications of medical treatment, electromagnetic (EM) compatibility, antenna pattern shaping, target stealth, etc.[1–6] Many efforts in the previous investigation about the absorber mainly concentrate on reducing its thickness, simplifying its configuration, and so on.[7] In most practical applications, there is an urgent need to develop an absorber responding to the EM wave with an adequately wide frequency band.[8] Therefore, researchers have developed some techniques to improve the operation bandwidth, such as pyramid[9] and metamaterials.[3–6] However, they may have a non-planar structure and be unsuitable for integration or limited in extending the frequency range.

Over the past few years, graphene, as a two-dimensional (2D) material, has been frequently investigated due to its exotic thermal, mechanical, optical, and electrical properties.[10–12] The surface impedance of graphene can be adjusted by chemical doping,[13] applying a bias voltage,[14] optical pump excitation,[15] and so on. Hence, graphene has been widely exploited in the design of various devices such as polarization polarizers,[16] sensors,[17] antennas,[18,19] SPPs waveguides,[20,21] and absorbers.[22–31] In the aspect of the absorber, there are frequency reconfigurable narrowband absorbers,[22,23] multi-frequency band absorbers,[24–26] and wideband absorbers with moderate bandwidths (e.g., the relative bandwidth (RBW) with absorption rate (AR) greater than 90% is less than 80%).[27–30] Obviously, those absorbers are still limited for their failure in covering a sufficiently wide frequency range directly. According to the literature, there have been two previous endeavors in realization of an ultra broadband absorber. In Ref. [31], an array of a graphene–dielectric structure with seven-layer frustum pyramids achieved a RBW of 170%, and in Ref. [32], a multilayered graphene absorber covering the RBW of 84.6% was introduced. However, both of them are polarization dependent due to the lack of four-fold rotational symmetry property about the propagation axis in unit structures.[33,34]

In this work, a design of ultra-broadband and polarization independent planar absorbers is proposed by introducing multilayered and symmetrical patterned graphene. The layers of graphene with proper surface impedance are separated by a dielectric substrate, and then the proposed absorber can well absorb an arbitrary polarized EM wave. In this design, the absorber with one-layer, two-layer, and three-layer graphene can achieve the RBW of 97.4%, 150.1%, and 165.3%, respectively. The operating frequency range directly covers the ultra broadband in the low-millimeter waveband regime (definitely, it is from the Ka band to the D band). The copper sheet at the bottom can be seen as a fully reflective ground. Between the graphene layers and the ground, the dielectric substrate is used to construct the absorber structure, which also forms a mutu-

*Project supported by the National Natural Science Foundation of China (Grant Nos. 61661012, 61461016, 61361005, and 61561013), the Natural Science Foundation of Guangxi, China (Grant No. 2017JJB160028), the Program for Innovation Research Team of Guilin University of Electronic Technology, China, and the Dean Project of Guangxi Key Laboratory of Wireless Wideband Communication and Signal Processing, China.

†Corresponding author. E-mail: ynjiang@guet.edu.cn

© 2017 Chinese Physical Society and IOP Publishing Ltd

ally coupled Fabry–Perot resonator to enhance the bandwidth.

The rest of this paper is arranged as follows. The surface impedance of graphene from K to D bands is presented in Subsection 2.1. In Subsection 2.2, the proposed multilayered absorber model is given. Then, in Subsection 2.3, the ultra-broadband and polarization independent absorptions are shown using commercial software CST Microwave Studio. In Subsection 2.4, the ultra-wideband absorption mechanism is illustrated using the destructive interference theory and multiple resonances. The relationships between the absorption and the other parameters are investigated in Subsection 2.5. Finally, the conclusions are drawn in Section 3.

2. Ultra broadband and polarization independent planar absorber

2.1. Surface impedance of graphene from K to D bands

As a 2D material with an atomically thin thickness, graphene can be characterized by surface conductivity,[35]

$$\sigma_s(\omega,\mu_c,\Gamma,T) = \sigma_{intra}(\omega,\mu_c,\Gamma,T) + \sigma_{inter}(\omega,\mu_c,\Gamma,T), \quad (1)$$

where σ_{intra} and σ_{inter} are the contributions from intraband and interband, respectively; ω, Γ, and T are the angular frequency, phenomenological scattering, and temperature, respectively; μ_c is the chemical potential and can be determined by either the applied bias electrostatic field or chemical doping. In frequency regimes from K to D bands, σ_{intra} is dominant and σ_{inter} can then be neglected. In addition, the surface impedance of graphene can be defined as[36]

$$Z_s(\omega,\mu_c,\Gamma,T) = 1/\sigma_s = R_s + jX_s. \quad (2)$$

For different μ_c, the frequency dependent surface impedances of undoped graphene with $T = 300$ K and $\Gamma = 5$ THz are shown in Fig. 1. For K to D bands, the following conclusions can be obtained: 1) the surface impedance decreases with increasing μ_c; 2) the surface resistance remains approximately constant for a fixed μ_c; and 3) the surface resistance is far greater than the surface reactance. From K to D bands, the stable feature of the graphene resistance with a fixed μ_c is very beneficial to the absorber achieving the ultra-broadband character.[27]

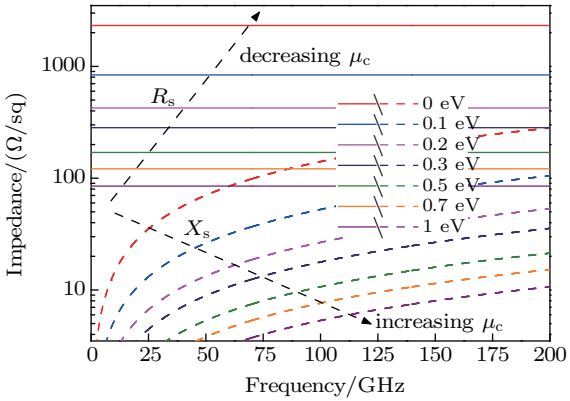


Fig. 1. Frequency dependent surface impedance of graphene for different chemical potentials.

2.2. Absorber with multilayered graphene

Here, we propose a design of an N-layer graphene absorber consisting of multi-scale rectangular graphene sheets (i.e., partial non-periodic planar structure). A schematic of the design with $N = 3$ is shown in Fig. 2. Figure 2(a) shows a model of an infinite planar absorber illuminated by a vertical incidence homogenous EM planar wave. The absorber consists of three-layer patterned graphene, a grounded copper with the conductivity of 5.8×10^7 S/m (the grounded copper can be seen as a fully reflective mirror from K to D bands), and three substrates each with a thickness of 0.7 mm and permittivity (ε_r) of 1.05. Due to the features of low dielectric constant, high strength, and thermal stability, polymethacrylimide (PMI) can be selected as the substrate.[37] A top view of the infinite planar absorber is displayed in Fig. 2(b). One can obviously see that there are three scales of graphene sheets and the absorber can be simulated by using the unit cell (as shown in Fig. 2(c)) truncated with periodic boundaries in CST Microwave Studio. The geometrical parameters of the unit cell are as follows: $a = 1.5$ mm, $g = 0.6$ mm, and $p = 5.7$ mm. The specific separated structure of the unit cell is shown in Fig. 2(d).

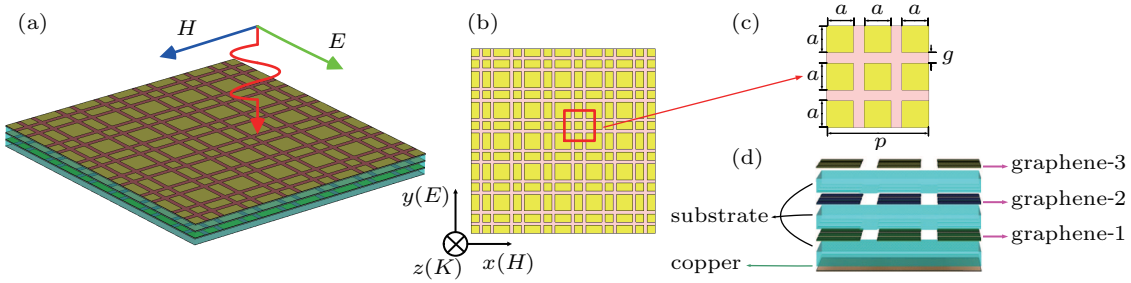


Fig. 2. Schematic of the designed absorber: (a) 3D model of an infinite planar absorbing screen illuminated by a vertical incidence homogenous EM planar wave; (b) top view of the absorber; (c) 2D unit structure used in CST simulation; and (d) the separated structure of the unit structure (from bottom to top, graphene is numbered with 1, 2, and 3, respectively).

2.3. Ultra-broadband and polarization independent absorption

The frequency dependent AR can be obtained as $A(f) = 1-R(f)-T(f)$ with reflection given by $R(f) = |S_{11}(f)|^2$ and transmission given by $T(f) = |S_{21}(f)|^2$ to measure the absorption performance of the absorber, where S_{11} and S_{21} are frequency dependent return losses and transmission losses, respectively. Because the copper ground prevents the propagation of an electromagnetic wave over the entire frequency range investigated,[38] the transmission is regarded as zero. Therefore $A(f) = 1-R(f)$.

Next, we investigate the properties of absorbing bandwidth and polarization sensitivity. By proper chemical doping, μ_c of graphene can be varied and therefore the surface impedances of graphene can be different. Based on the space match theory,[19,30] the absorption bandwidth can reach its maximum when the impedance of graphene is matched to that of free space (i.e., $Z_0 = 120\pi$). In this proposal, a consistent impedance or μ_c is adopted for all graphene sheets with different scales at the same layer, which is convenient for possible future manufacture.

For elaboration convenience, the serial number of the layered graphene from top to bottom monotonically decreases from N to 1, and the copper ground can be set as 0. Here, we assume μ_c of graphene distributed on the l-th interface is μ_{cl}. By optimizing μ_{cl} ($l = 1-N$) ($\mu_{c1} = 0.5$ eV; $\mu_{c1} = 0.5$ eV, $\mu_{c2} = 0.34$ eV; and $\mu_{c1} = 0.5$ eV, $\mu_{c2} = 0.34$ eV, $\mu_{c3} = 0.326$ eV for absorber structures with $N = 1$, 2, and 3), the maximum operating bandwidths of 51.4–149 GHz, 25.4–178.3 GHz, and 17.9–188.7 GHz (i.e., the RBWs of 97.4%, 150.1%, and 165.3%) can be obtained, as shown in Fig. 3. One can find that the AR bandwidth is steadily broadened with increasing N, and the absorber with $N = 3$ covers all the bands of K, Ka, U, V, W, and D. The aforementioned μ_{cl}, corresponding surface impedance of graphene, and bandwidths of the absorber are listed in Table 1. From Fig. 2 and Table 1, we can further discover the fourfold rotational symmetry in the unit structure about the z-axis, and then the designed absorber is polarization independent for the vertical incident wave, as shown in Fig. 3. It should be noted that the total thickness of the absorber varies with N, the total thicknesses are respectively 0.7 mm, 1.4 mm, and 2.1 mm for $N = 1$, 2, and 3 if there is no special prompt in this paper.

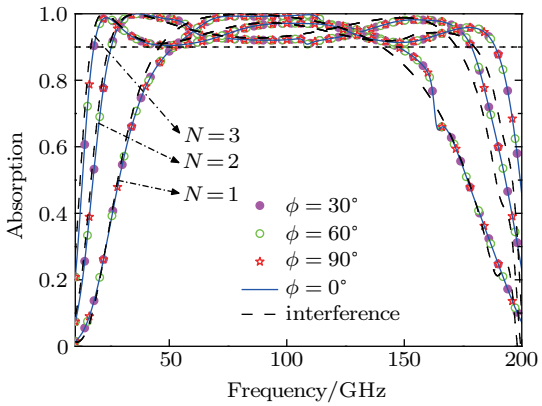


Fig. 3. (color online) Simulated absorption (bandwidth and polarization-independence) for the proposed absorber with $N = 1$, 2, and 3. ϕ is the linear polarization angle (i.e., the angle between the electric field component of the incident wave and $+x$ axis).

Table 1. Parameters of graphene and the absorption bandwidths.

N	1st layer		2nd layer		3rd layer		Effective bandwidth/GHz	RBW
	μ_{c1}/eV	$Z_1/(\Omega/\square)$	μ_{c2}/eV	$Z_2/(\Omega/\square)$	μ_{c3}/eV	$Z_3/(\Omega/\square)$		
1	0.5	170	–	–	–	–	51.4–149.0	97.4%
2	0.5	170	0.34	250	–	–	25.4–178.3	150.1%
3	0.5	170	0.34	250	0.325	260	17.9–188.7	165.3%

2.4. Ultra-broadband absorption mechanism

In this section, both destructive interference theory and multiple resonances approach are employed to explain the physical mechanism of ultra-broadband absorption of the proposed design.

2.4.1. Destructive interference theory

The side view of the incidence, reflection, and transmission paths of EM wave in the N-layer absorber is displayed in Fig. 4(a). The mechanism of absorption can be explained by using the destructive interference theory,[38–40] i.e., the destructive interference between the direct reflection and the following multiple emergent waves that effectively traps the wave in the multilayered absorber, and then results in the high absorption. The total reflection coefficient at the l-th interface can be expressed as

$$\Gamma_l = r_{l,l-1} + \frac{t_{l,l-1}t_{l-1,l}\Gamma_{l-1}\,\mathrm{e}^{-\mathrm{i}2\phi_l}}{1 - r_{l-1,l}\Gamma_{l-1}\,\mathrm{e}^{-\mathrm{i}2\phi_l}} = r_{l,l-1} + T_{l-1,l}, \quad (3)$$

where the number of interfaces l is from 1 to N, $\phi_l = kn_l d_l$ represents the k-th delayed phase across the dielectric substrate with thickness d_l and refractive index $n_l = \sqrt{\varepsilon_r}$, $t_{l,l-1}$, $t_{l-1,l}$ and $r_{l,l-1}$, $r_{l-1,l}$ respectively represent the transmission and reflection coefficients across the l-th interface, and $T_{l-1,l}$ represents the following multiple emergent waves resulting from the superposition of the multiple reflections in the structure on the right side of the l-th interface. The copper acting as a ground does not permit waves to transmit, such that $t_{0,-1} = 0$ and $r_{0,-1} = -1$, therefore $\Gamma_0 = r_{0,-1} = -1$ can be derived from

Eq. (3). By forward iteration, Γ_N can be obtained, and the AR can also be obtained as $A(f) = 1 - |\Gamma_N|^2$. Under ideal conditions of amplitude (i.e., $|r_{N,N-1}| = |T_{N-1,N}|$) and phase difference (i.e., $\alpha = |\arg(r_{N,N-1}) - \arg(T_{N-1,N})| = \pi$), an ideal AR (i.e., AR = 100%) would be obtained, which satisfies the strongest destructive interference of the electromagnetic field. Even though $|r_{N,N-1}| = |T_{N-1,N}|$ and $\alpha = \pi$ are not strictly satisfied simultaneously, an AR of 90% can also be achieved.

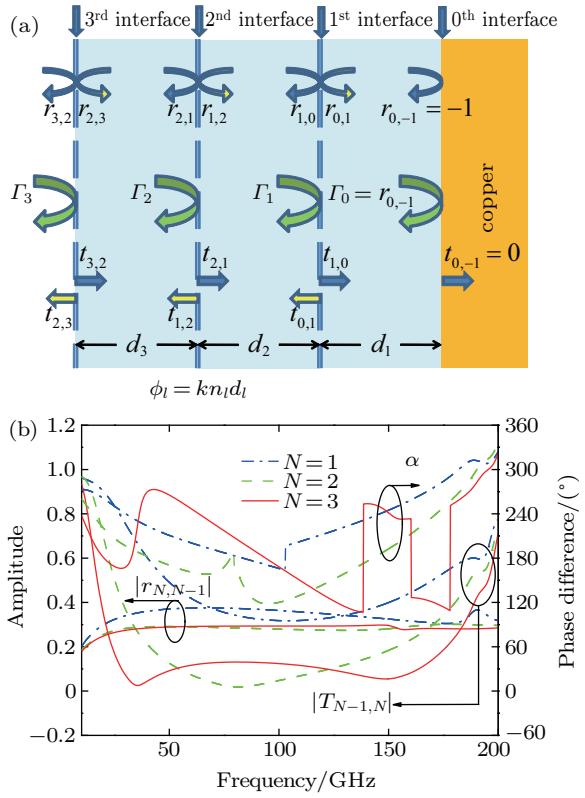


Fig. 4. (color online) (a) A schematic diagram of the transmission and reflection for the structure with $N = 3$. (b) The amplitude and phase difference of direct reflection and multiple reflections for different N.

The magnitude of the direct reflected wave at the N-th interface and the multiple emergent waves, and the phase difference between them for the N-layer graphene absorber are described in Fig. 4(b). For $N = 1$, $|r_{N,N-1}|$ and $|T_{N-1,N}|$ are comparable and the phase difference α is approximately 180° in the frequency range from 51.4 GHz to 149 GHz. Despite larger difference between $|r_{N,N-1}|$ and $|T_{N-1,N}|$ for $N = 2$ than that for $N = 1$, the phase difference α is much closer to 180° from 25.4 GHz to 178.3 GHz, which makes the two-layer graphene absorber have a more excellent AR bandwidth. Comparing with $N = 2$, the AR performance further improves due to the smaller difference between $|r_{N,N-1}|$ and $|T_{N-1,N}|$ and comparable phase difference α when $N = 3$. The AR for the proposed absorber with different N can also be calculated by the interference theory, as shown by the dashed line in Fig. 3(a), and an excellent agreement is obtained between CST simulations and the results of interference theory.

2.4.2. Multiple resonances approach

A single-layer graphene absorber is based on a Salisbury screen absorber and presents essential Fabry–Perot resonance[24]

$$f_m = c\frac{2m-1}{4nH}, \tag{4}$$

where n and H are respectively the refractive index and thickness of the dielectric substrates, and c and f_m are the phase velocity along the z direction in free space and the resonant frequency with mode index m, respectively. The incident waves and reflected waves have opposite phase differences at f_m, which leads to periodic reflection zeros and absorption peaks. Here, we assume N of the proposed absorber is 1, but the thickness H of the dielectric substrate is d_1 (0.7 mm), $d_1 + d_2$ (1.4 mm), and $d_1 + d_2 + d_3$ (2.1 mm), respectively, and the impedance Z of graphene is correspondingly Z_1, Z_2, and Z_3 (see Table 1). The Fabry–Perot resonant frequencies are listed in Table 2. Meanwhile, their CST simulations are also provided, as shown in Fig. 5(a). We can obviously see that the positions of the resonant frequencies simulated by CST Microwave Studio are consistent with those calculated by Fabry–Perot resonance.

Table 2. Fabry–Perot resonant frequencies (GHz). The resonant frequencies are not within the frequency range from K to D bands when $H = d_1$ with $k = 2$ and 3 and $H = d_1 + d_2$ with $k = 3$.

Mode index m	H		
	d_1	$d_1 + d_2$	$d_1 + d_2 + d_3$
1	104.6	52.3	34.9
2	313.7	156.8	104.6
3	522.8	261.4	174.3

Furthermore, $N = 2$ and $N = 3$ are studied. For $N = 2$, there are three cases, i.e., there are no graphene-3, graphene-2, and graphene-1 with the thickness H of $d_1 + d_2$, $d_1 + d_2 + d_3$, and $d_1 + d_2 + d_3$, respectively. Their S_{11} are also provided in Fig. 5(a). We can conclude that the resonance of an absorber with multilayered graphene is caused by the combination of multiple absorbers with corresponding single layer graphene. For example, the S_{11} under the condition of $N = 2$ with no graphene-3 ($H = d_1 + d_2$) can be seen as a combination of the S_{11} of an absorber only with graphene-1 and that of an absorber only with graphene-2; S_{11} of the proposed absorber with $N = 3$ is the combination of S_{11} of three absorbers only with graphene-1, graphene-2, and graphene-3, respectively. The multiple resonant frequencies are brought closer and combine into the ultra-broadband absorption of the proposed multilayered graphene-based absorber.

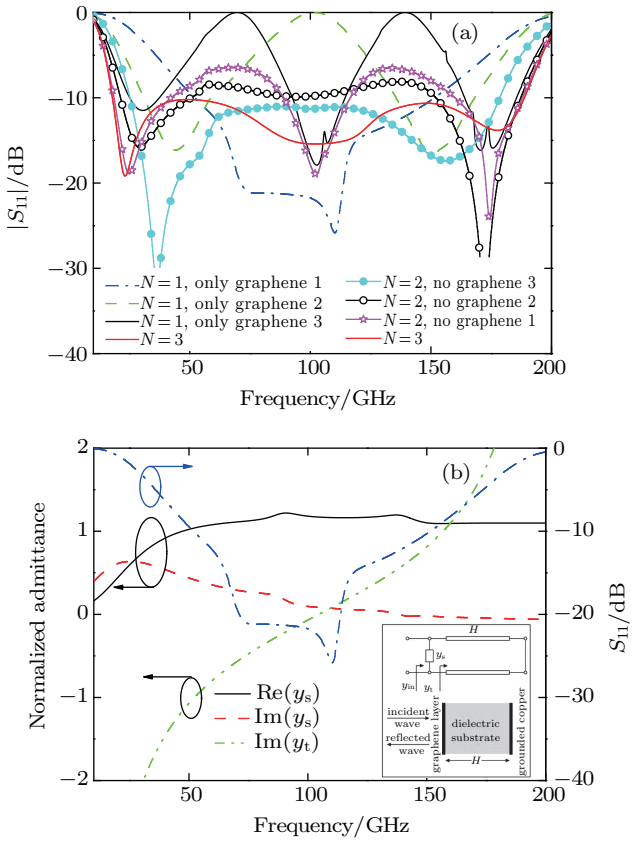


Fig. 5. (a) Simulated S_{11} of the proposed absorber with different N and different thickness of dielectric substrates. (b) Normalized component admittances and simulated S_{11} for $N = 1$ and $H = d_1$.

When $N = 1$ and $H = d_1$, the absorber also shows the ultra-broadband absorption (RBW is 97.4%), which can be explained by the transmission line model.[30] The transmission line model is shown in the inset of Fig. 5(b), where y_t indicates the normalized admittance (i.e., admittance is normalized by characteristic admittance of free space $Y_0 = 1/Z_0$) deriving from a short circuit (i.e., grounded copper) transformed by the dielectric substrate with thickness H, y_s represents the equivalent normalized admittance of the graphene layer, and the total normalized admittance $y_{in} = y_t + y_s$. At ~ 104.6 GHz, Im(y_s) and Im(y_t) are approximate and about 0, which makes Im(y_{in}) approximately equal to 0, and therefore there is a strong resonance peak at this frequency. Moreover, Im(y_s) and Im(y_t) are basically two opposite numbers in the frequency range from ~ 70 GHz to ~ 100 GHz, a resonant waveband with $|S_{11}| \leq -20$ dB is obtained when Im(y_{in}) ≈ 0 and Re(y_{in}) = Re(y_s) ≈ 1. Both strong resonances within the frequencies from ~ 70 GHz to ~ 100 GHz and at ~ 104.6 GHz are brought closer, and the ultra broadband (from 51.4 GHz to 149.0 GHz) performance with AR greater than 90% (i.e., $|S_{11}| \leq -10$ dB) is then achieved (shown by the blue dashed line).

2.5. Discussion

In this section, we firstly investigate the relationship between the absorption and substrate parameters (its thickness and permittivity) for the proposed absorber with $N = 1$ and $H = d_1$, and then the influence of the incident angle is studied for $N = 3$.

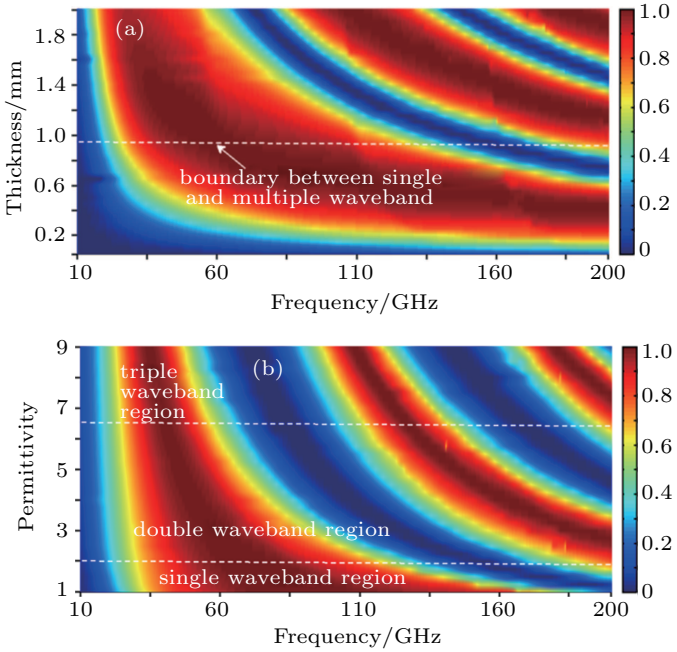


Fig. 6. Absorption as a function of frequency and two parameters of the dielectric substrate for the proposed absorber with $N = 1$: (a) thickness, (b) permittivity.

2.5.1. Substrate parameters dependent absorption

When $N = 1$ and $H = d_1$, the relationship between the absorption and the thickness of the dielectric substrate is displayed in Fig. 6(a), where the thickness H varies from 0.05 mm to 2 mm. It can be observed that the absorber with $H \leq 0.95$ mm operates in an ultra-wideband with AR greater than 90%. However, the absorption spectra present double bands and even triple bands when $H \geq 0.95$ mm. In fact, these extra absorption bands correspond to higher modes with mode index $m \geq 2$ in Eq. (4). Moreover, a red shift emerges for all absorption bands with increasing H, which is due to the quarter-wavelength intrinsic property satisfying the Fabry–Perot resonance condition. From Fig. 6(a), we obtain that the value of H can be selected to maximize the absorption bandwidth, where $H = 0.7$ mm provides the maximum RBW of 97.4%.

The dielectric substrate plays an important role, for example, supporting the graphene-based structure with grounded copper and formatting the Fabry–Perot resonator. Its ε_r also affects the absorption performance. For $N = 1$ and $H = d_1$, the relationship between the absorption and ε_r is displayed in Fig. 6(b), where ε_r varies from 1.0 to 9.0. Attributing to the appearance of the absorption bands with higher m modes, the absorber operates in the states of single, double, and triple waveband for $\varepsilon_r \leq 2$, $2 < \varepsilon_r \leq 6.5$, and $\varepsilon_r > 6.5$, respectively.

In addition, the operating wavebands exhibit red shift with increasing ε_r because n in Eq. (4) is increased accordingly. For $\varepsilon_r = 1$, the maximum RBW with AR greater than 90% is achieved, it is just like a vacuum but it cannot support the structure. Hence, the Rohacell PMI foam with high strength and permittivity $\varepsilon_r = 1.05$ can be selected.[37]

2.5.2. Influence of incident angles

The dependent characteristic on the incident angles is closely related to the performance of the absorber. When $N = 3$, the frequency dependence absorption for different incident angles (i.e., θ, the angle between the z axis and wave vector $\boldsymbol{K}$ in the xoz plane) of the designed absorber is shown in Fig. 7, in which both TM polarization and TE polarization are given. For TM and TE polarizations, the electric field components of the incident wave are respectively parallel and perpendicular to the xoz plane. The absorption waveband for TM polarization exhibits a blue shift with increasing θ but the RBW with AR greater than 90% has no significant change. For TE polarization, the AR is steadily worse but it is still greater than 80% even if $\theta = 60°$. The RBW with AR greater than 80% increases with the increase of θ due to the blue shift of the upper limit frequency and the constant of the lower limit frequency. It is believed that our absorbers can respond to an incoming wave within a wide angle range. The reason for a blue shift for both polarizations is that the phase velocity along the z direction (i.e., c in Eq. (4)) increases with increasing θ.

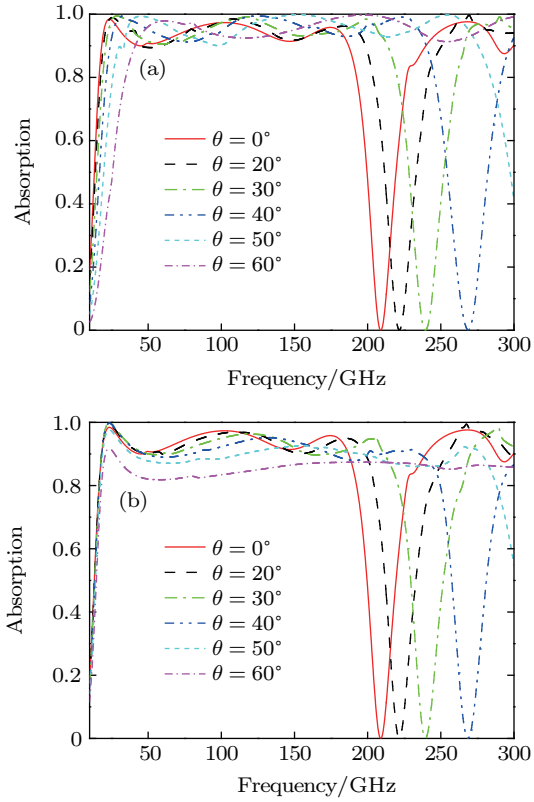


Fig. 7. (color online) Influence of the incident angles on the proposed absorber with $N = 3$: (a) TM polarization, (b) TE polarization.

3. Conclusion

In the frequency range of K to D bands, an ultra-broadband and polarization-independent planar absorber based on multilayered graphene structure has been proposed. The RBW can be enhanced by increasing N and the RBWs with AR greater than 90% of the proposed absorbers with $N = 1$, 2, and 3 are 97.4%, 150.1%, and 165.3%, respectively. The physical mechanism of the ultra-broadband absorption is elaborated upon using the destructive interference theory and multiple resonances approach. Moreover, the absorber is polarization independent due to its fourfold rotational symmetry in the unit structure. Simulations show that the absorber also holds the properties of wide angle range absorption. The proposed multilayered graphene absorber will obtain extensive applications in military and civilian areas.

Acknowledgement

We thank Dr. Zhirun Hu from the University of Manchester for his suggestions.

References

[1] Titt U, Mirkovic D, Sawakuchi G O, Perles L A, Newhauser W D, Taddei P J and Mohan R 2010 *Phys. Med. Biol.* **55** 7097
[2] Cheng Q, Cui T J, Jiang W X and Cai B G 2010 *New J. Phys.* **12** 063006
[3] Ma H F and Cui T J 2010 *Nat. Commun.* **1** 21
[4] Park J W, Tuong P V, Rhee J Y, Kim K W, Jang W H, Choi E H, Chen L Y and Lee Y P 2013 *Opt. Express* **21** 9691
[5] Wang B X, Wang L L, Wang G Z, Huang W Q, Li X F and Zhai X 2014 *Appl. Phys. A* **115** 1187
[6] Wang B X and Wang G Z 2017 *Appl. Phys. Express* **10** 034301
[7] Ra'di Y, Simovski C R and Tretyakov S A 2015 *Phys. Rev. Appl.* **3** 037001
[8] Gill N, Puthucheri S, Singh D and Agarwala V 2017 *J. Mater. Sci.: Mater. Electron.* **28** 1259
[9] Lv S P, Liu S H and Zhao Y B 2005 *Mater. Technol.* **20** 211
[10] Geim A K and Novoselov K S 2007 *Nat. Mater.* **6** 183
[11] Novoselov K S, Falko V I, Colombo L, Gellert P R, Schwab M G and Kim A K 2012 *Nature* **490** 192
[12] Ferrari A C, Bonaccorso F, Fal'ko V, *et al*. 2015 *Nanoscale* **7** 4598
[13] Geng H Z, Kim K K, So K P, Lee Y S, Chang Y and Lee Y H 2007 *J. Am. Chem. Soc.* **129** 7758
[14] Ren L, Zhang Q, Yao J, Sun Z, Kaneko R, Yan Z, Jin Z, Kawayama I, Tonouchi M, Tour J M and Kono J 2012 *Nano Lett.* **12** 3711
[15] Li Q, Tian Z, Zhang X, Singh R, Du L, Gu J, Han J and Zhang W 2015 *Nat. Commun.* **6** 7082
[16] Yu X, Gao X, Qiao W, Wen L and Yang W 2016 *IEEE Photonic. Tech. L.* **28** 2399
[17] Kulkarni G S, Reddy K, Zhong Z and Fan X 2014 *Nat. Commun.* **5** 4376
[18] Aldrigo M, Dragoman M and Dragoman D 2014 *J. Appl. Phys.* **116** 114302
[19] Jiang Y N, Yuan R, Gao X, Wang J, Li S M and Lin Y Y 2016 *Chin. Phys. B* **25** 118402
[20] Vakil A and Engheta N 2011 *Science* **332** 1291
[21] Yuan L, Yan X, Wang Y, Sang T and Yang G 2016 *Appl. Phys. Express* **9** 092202
[22] Huang X, Zhang X, Hu Z, Aqeeli M and Alburaikan A 2015 *IET Microw. Antenna. P.* **9** 307
[23] Xu B, Gu C, Li Z and Niu Z 2013 *Opt. Express* **21** 023803
[24] Wu B, Tuncer H M, Naeem M, Yang B, Cole M T, Milne W I and Hao Y 2014 *Sci. Rep.* **4** 4130
[25] Xu B, Gu C, Li Z and Niu Z 2014 *IEEE Antennas Wireless Propag. Lett.* **13** 822

[26] Kong X, Shi X, Mo J and Liu S 2017 *Opt. Commun.* **383** 391
[27] Huang X, Hu Z and Liu P 2014 *AIP Adv.* **4** 117103
[28] Andryieuski A and Lavrinenko A V 2013 *Opt. Express* **21** 9144
[29] Zhu Z, Guo C, Zhang J, Liu K, Yuan X and Qin S 2015 *Appl. Phys. Express* **8** 015102
[30] Olszewska-Placha M, Salski B, Janczak D, Bajurko P R, Gwarek W and Jakubowska M 2015 *IEEE Trans. Antennas Propag.* **63** 565
[31] He S and Chen T 2013 *IEEE T. Thz. Sci. Techn.* **3** 757
[32] Amin M, Farhat M and Bağcı H 2013 *Opt. Express* **21** 29938
[33] Landy N I, Bingham C M, Tyler T, Jokerst N, Smith D R and Padilla W J 2009 *Phys. Rev. B* **79** 125104
[34] Padilla W J, Aronsson M T, Highstrete C, Lee M, Taylor A J and Averitt R D 2007 *Phys. Rev. B* **75** 041102
[35] Hanson G W 2008 *J. Appl. Phys.* **103** 064302
[36] Aldrigo M, Dragoman M, Costanzo A and Dragoman D 2013 *J. Appl. Phys.* **114** 184308
[37] Costa F, Monorchio A and Manara G 2010 *IEEE Trans. Antennas Propag.* **58** 1551
[38] Wang J and Jiang Y 2017 *Opt. Express* **25** 5206
[39] Chen H T 2012 *Opt. Express* **20** 7165
[40] Jiang Y N, Wang Y, Ge D B, Li S M, Cao W P, Gao X and Yu X H 2016 *Acta Phys. Sin.* **65** 054101 (in Chinese)